Analyst

Dynamic Article Links

Cite this: *Analyst*, 2012, **137**, 5614

www.rsc.org/analyst

PAPER

Wash-less and highly sensitive assay for prostate specific antigen detection

Ghadeer A. R. Y. Suaifan,[a] Chiheb Esseghaier,[b] Andy Ng[b] and Mohammed Zourob*[b]

Received 3rd September 2012, Accepted 24th September 2012
DOI: 10.1039/c2an36243k

A novel, simple and facile biosensor for prostate specific antigen (PSA) detection was constructed. In this method, proteolytically active PSA is capable of cleaving PSA substrate–magnetic carrier complexes. Electrochemical analysis of the sensor layer showed a significant decrease in impedance signal after proteolysis has occurred, whereas a positive change in impedance was observed using a negative control substrate, indicating the specificity of our detection mechanism. The biosensor has the ability to monitor PSA concentrations ranging from 1 pg ml^{-1} to 1 μg ml^{-1} with a detection limit as low as 1 pg ml^{-1}. The sensor offers the possibility of developing a wash-less and cost-effective point-of-care device due to the simplicity of the probe immobilization process and the elimination of labeling and reporter molecules during the biosensing step.

1. Introduction

Cancer is the second most common cause of death in the United States, exceeded only by heart disease. In males, prostate carcinoma is the leading cause of cancer-related deaths, aside from lung cancer.[1–3] During prostate cancer screening, the PSA level for healthy individuals is usually reported to be below 4×10^3 pg ml^{-1}. However, when the PSA level is $\geq 10^4$ pg ml^{-1}, a high probability of prostate cancer is indicated. Indeed, the concentration range between 4×10^3 and 10^4 pg ml^{-1} is considered as a 'gray diagnostic zone'.[4] Prostate specific antigen (PSA) is a 30 kDa kallikrein-like serine protease produced by both normal prostate epithelial cells and prostate cancer cells.[5–7] There are two types of PSA in body fluids, the proteolytically active PSA and the inactive PSA, of which the proteolytically active PSA is found to be a useful diagnostic serological marker for the early diagnosis and monitoring of prostate cancer.[8–10]

Radical prostatectomy is often used to eradicate prostate carcinoma. However, biochemical evidence of recurrent prostate carcinoma may be seen in approximately 40% of patients 15 years after surgery.[11] More importantly, in recurrent prostate carcinoma, an increase in PSA occurs nearly universally.[12] It has been proven that prostate cancer relapse could be identified approximately 1 year earlier in most patients with recurrence if a PSA assay is capable of offering a detection limit of <100 pg ml^{-1}.[13,14] Therefore, a facile and sensitive PSA detection method represents one of the most promising approaches toward cancer reduction and so improving the survival rate.

Currently, most PSA detection methods are based on immunoassays including fluorescence,[1,15] absorption[4] and electrochemical[16,17] approaches. Commercial immunoassays for total PSA analysis include Abbott IMX[18] and Hybritech Tandem E and R.[19] Furthermore, PSA analysis can be performed with UBI Magiwel[20] and Alpco Diagnostics.[21] In general, these detection methods offer good sensitivity but are either time-consuming, expensive, complicated, not reproducible or cannot discriminate between the active and inactive PSA.[1] Therefore, there is a distinct need for the development of a simple, facile, inexpensive, highly sensitive (detection limit approaching 1 pg ml^{-1}) and reproducible method for the detection of proteolytically active PSA for detecting biochemical relapse after radical prostatectomy.

The present work describes the development of simple, wash-less and inexpensive electrochemical impedimetric PSA sensor. In this detection method, the probe consists of a specific PSA substrate peptide immobilized on a magnetic bead *via* covalent binding upon coupling through its N-terminus and is attached onto the gold sensor surface at the C-terminus. This construct results in a layer of magnetic beads close to the sensor surface. Upon cleavage of the probe peptide by PSA, the physical link between the magnetic beads and the sensor surface will be abolished. An external magnetic field will collect the cleaved magnetic beads from the sensor surface as a result of protease-induced cleavage, which in turn will result in a significant shift of the electrochemical signal (Fig. 1). This label-free detection does not require a washing or blocking step and offers high specificity and sensitivity.[22] This very simple biosensing mechanism could be employed for lab-on-a-chip (LOC) biosensor elaboration and will lead to an efficient and reliable means of detecting clinically biochemical relapse of prostate carcinoma after radical prostatectomy.

[a]*Department of Pharmaceutical Sciences, Faculty of Pharmacy, The University of Jordan, Amman, 11942-Jordan*
[b]*Institut national de la recherche scientifique, Centre – Energie Matériaux Télécommunications, 1650, Boul. Lionel Boulet, Varennes, Québec, J3X 1S2, Canada. E-mail: zourob@emt.inrs.ca; Fax: +1-450 929-8102; Tel: +1-514-228-6981*

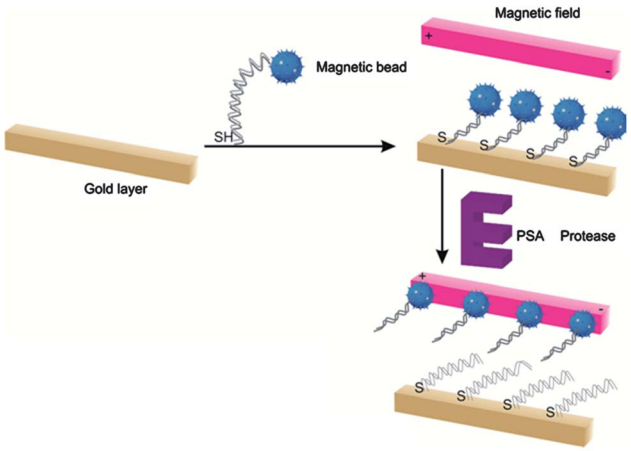

Fig. 1 Mechanism of PSA protease detection on the gold sensor surface.

2. Experimental

2.1. Materials and reagents

Carboxyl-terminated beads of 30 nm diameter suspended in a storage buffer (10 mM Tris base, 0.15 M NaCl, 0.1% (w/v) bovine serum albumin (BSA), 1 mM ethylenediaminetetraacetic acid (EDTA), 0.1% sodium azide, pH 7.5) were provided by TurboBeads (Switzerland). Recombinant prostate-specific antigen was purchased from Sigma-Aldrich (Ontario, Canada). The peptide sequences (substrate peptide 1: GSGSGSG SEHSSKLQLAKGSGSGSGSC; substrate peptide 2: GSGSGS GSKALQLKSSHEGSGSGSGSC; control: GGGSGSGSARV LAEAGGGSGSGSC) were synthesized at the Sheldon Biotechnology Center at McGill University (Montreal, Canada). The coupling agent 1-ethyl-3(3-dimethylaminopropyl) carbodiimide (EDC) and *N*-hydroxysuccinimide (NHS) were purchased from Sigma (Ontario, Canada). The coupling buffer (10 mM potassium phosphate, 0.15 M NaCl, pH 5.5) and wash/storage buffer were prepared from chemicals of analytical grade. The PBS buffer used for all electrochemical measurements was composed of 0.1 mM Na_2HPO_4, 1.8 mM KH_2PO_4, 1.4 mM NaCl, and 2.7 mM KCl.

2.2. Conjugation of the prostate-specific antigen substrate peptide to magnetic beads

The magnetic beads suspension (1 ml) was mixed with each peptide (1.0 mg ml^{-1}), coupling agent EDC (0.57 mg ml^{-1}) and NHS (12 μg ml^{-1}) with gentle shaking at room temperature for 24 hours. The uncoupled peptides were removed by washing the beads 3 times using wash buffer. Finally, the beads were stored at 4 °C in storage buffer.

2.3. Electrode preparation and probe immobilization

The gold electrode surface was polished using alumina 0.05 μm for 20 min, incubated in ultra-pure water and placed in an ultrasonic bath for 5 min. The electrode was then immersed in a freshly prepared piranha solution (1 : 2, H_2O_2 : H_2SO_4) for 2 min and washed with ultra-pure water. Subsequently, cyclic voltammetry in 0.1 M H_2SO_4 was applied to the bare gold surface with a potential ranging from 0 to 1.6 V using a scan rate of 100 mV s^{-1} for 30 rounds to ensure complete removal of micro-pollutants through successive oxidation and reduction of the gold surface. Finally, the cleaned gold electrode was immersed overnight in the magnetic bead–peptide solution at room temperature, washed with PBS buffer and then placed in the electrochemical cell for subsequent measurements.

2.4. Electrochemical characterizations

An Autolab potentiostat/galvanostat was used in order to perform cyclic voltammetry and electrochemical impedance spectroscopy techniques. The bare and modified gold surfaces were analysed using cyclic voltammetry with a potential ranging from −0.3 to 0.6 V and a scan rate of 100 mV s^{-1}. Electrochemical impedance spectroscopy was also applied at the potential of 0.25 V in the frequency range of 100 mHz to 50 kHz in order to characterize the magnetic bead–peptide deposition and to perform PSA detection. All experiments were carried out in a closed electrochemical cell inside a Faraday cage. The electrochemical cell is composed of a working electrode (gold electrode), a reference electrode (Ag/Ag^+) and a control platinum electrode. The magnet is permanently attached at the bottom of the cell in order to attract free magnetic beads liberated during the enzymatic cleavage reaction. The number of cycles in each experiment was adjusted according to the stability of the electrochemical signal. The NOVA software allows real-time visualization of the electrochemical signal variation as well as data acquisition and processing.

2.5. Biosensing of PSA

Different concentrations of PSA (0.1 pg ml^{-1}, 1 pg ml^{-1}, 10 pg ml^{-1}, 10^2 pg ml^{-1}, 10^3 pg ml^{-1}, 10^4 pg ml^{-1}, 10^5 pg ml^{-1} and 10^6 pg ml^{-1}) were applied onto the recognition peptide monolayer of the sensor. Each cleavage reaction was monitored through real-time measurement of the change in the couple resistance/capacitance of the Nyquist plot. Modeling and theoretical calculation, as well as Nyquist and cyclic voltammetry plots were produced with the NOVA software. Calibration plots were established based on the values generated by the fitting calculations of the experimental curves.

3. Results and discussion

Electrochemical impedance spectroscopy is an attractive analytical method for the detection of various biomarkers due to its ability to probe bio-chemical interactions occurring near the recognition area of the electrode surface with high sensitivity and simplicity.[23,24] The same technique can also be applied for the characterization of the electrode surface. Indeed, microscopic structural changes of the electrode surface due to the deposition of materials would induce a significant variation in their electrochemical behavior towards the electrical charges present inside the measurement buffer.[25] For this reason, we used faradic impedance spectroscopy in order to take advantage of the application of redox ions ($Fe(CN)_6^{3-}/Fe(CN)_6^{4-}$) as a biocompatible electrochemical probe.

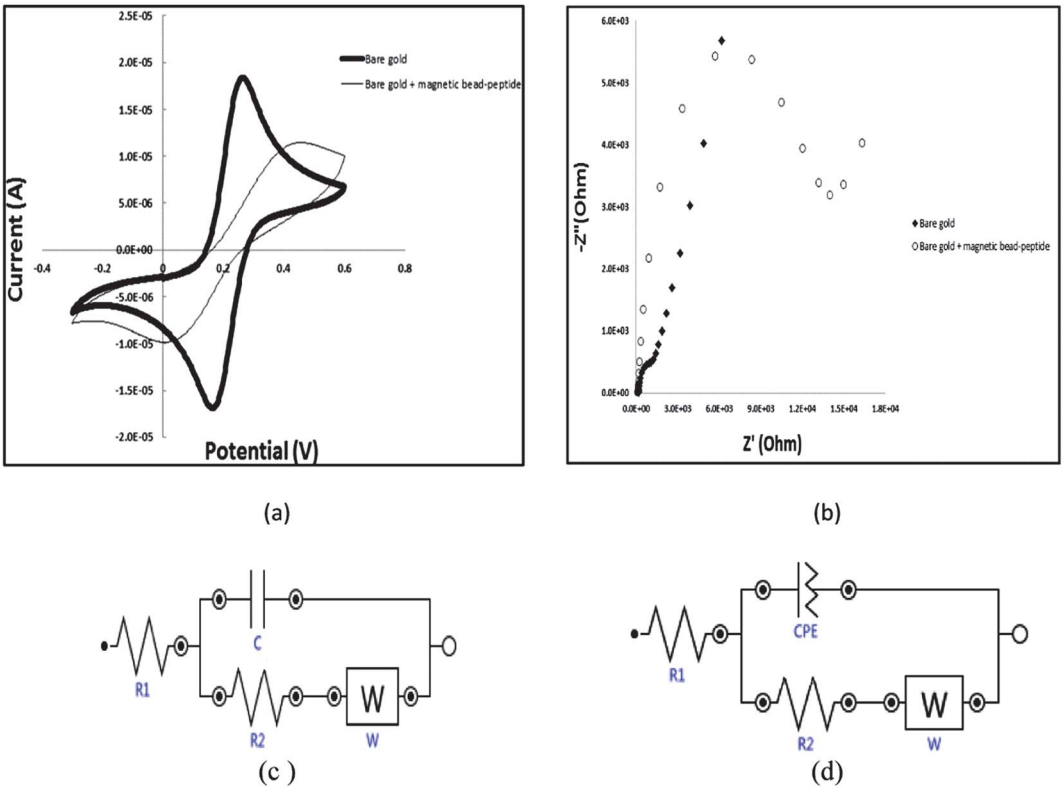

Fig. 2 Cyclic voltammogram (a) and Nyquist plots (b) of the bare gold and bio-functionalized gold surfaces; (c) equivalent circuit of the bare gold electrode and (d) equivalent circuit of the modified gold electrode.

3.1. Immobilization of the peptidic probe

We applied cyclic voltammetry and electrochemical impedance spectroscopy (EIS) in order to characterize the bare and modified gold electrode surfaces. Fig. 2a shows a significant drop in the oxidation and reduction peaks of the ferrocyanide redox couple ($Fe(CN)_6^{3-}/Fe(CN)_6^{4-}$) with respect to the bare gold, indicating a partial faradic current blocking effect of ion diffusion due to the presence of the magnetic bead–peptide layer on the gold surface. The impedimetric characterization was in good agreement with the cyclic voltammetry results. We were able to recognize a marked increase in the Nyquist curve diameter as well as a significant decrease in the Warburg diffusion after incubation of the bare gold in the magnetic bead–peptide solution (Fig. 2b). These findings provided evidence for the covalent bonding of the PSA substrate peptide with the bare gold through the sulfur atom of the C-terminal cysteine. Indeed, it has been proven that the gold–sulfur atom interaction is highly stable[26] which allows the establishment of a self assembled monolayer (SAM) of peptide labeled with magnetic beads. The formation of the magnetic bead–peptide monolayer can significantly perturb the reduction and oxidation reactions of the ferrocyanide and ferricyanide ions. The theoretical calculation of the experimental curves shows also a difference regarding the electrical model adopted for fitting purposes. In fact, the equivalent circuit corresponding to the bare gold includes the ohmic resistance of the electrolyte solution ($R1$), the pure capacitance (C), the Warburg impedance ($W1$) and the charge transfer resistance ($R2$), whereas, for the functionalized gold surface, the pure capacitance was changed with a constant phase element (CPE). This modification was made in order to consider the increase in the roughness due to the non-homogenous quality of the deposited layer[27] (Fig. 2c and d).

3.2. PSA biosensing

3.2.1. Detection of proteolytically active PSA. The introduction of different concentrations of PSA onto the functionalized gold surface induced a gradual decrease in the charge transfer resistance. Fig. 3a shows a significant drop in the Nyquist plot diameters with increasing concentrations of enzyme. It was possible to fit the electrochemical signals corresponding to the modified gold electrode with an equivalent circuit composed of 2 resistances, 2 capacitances and Warburg impedance components (Fig. 2d).

The decrease in charge transfer resistance was also observed with another peptide sequence containing a PSA cleavage site (Fig. 3b). The decrease in charge transfer resistance can be explained by the change in the structure and the conformation of our self-assembled monolayer upon PSA cleavage. The cleavage of the peptide sequence led to the release of magnetic beads and subsequently their attraction towards the magnet. The dissociation of magnetic beads from the electrode surface caused the destabilization of the blocking organic/metallic monolayer, resulting in an enhancement of the charge transfer rate of the ($Fe(CN)_6^{3-}/Fe(CN)_6^{4-}$) oxido–reduction reactions and a decrease in the impedance signals. In the absence of PSA, no

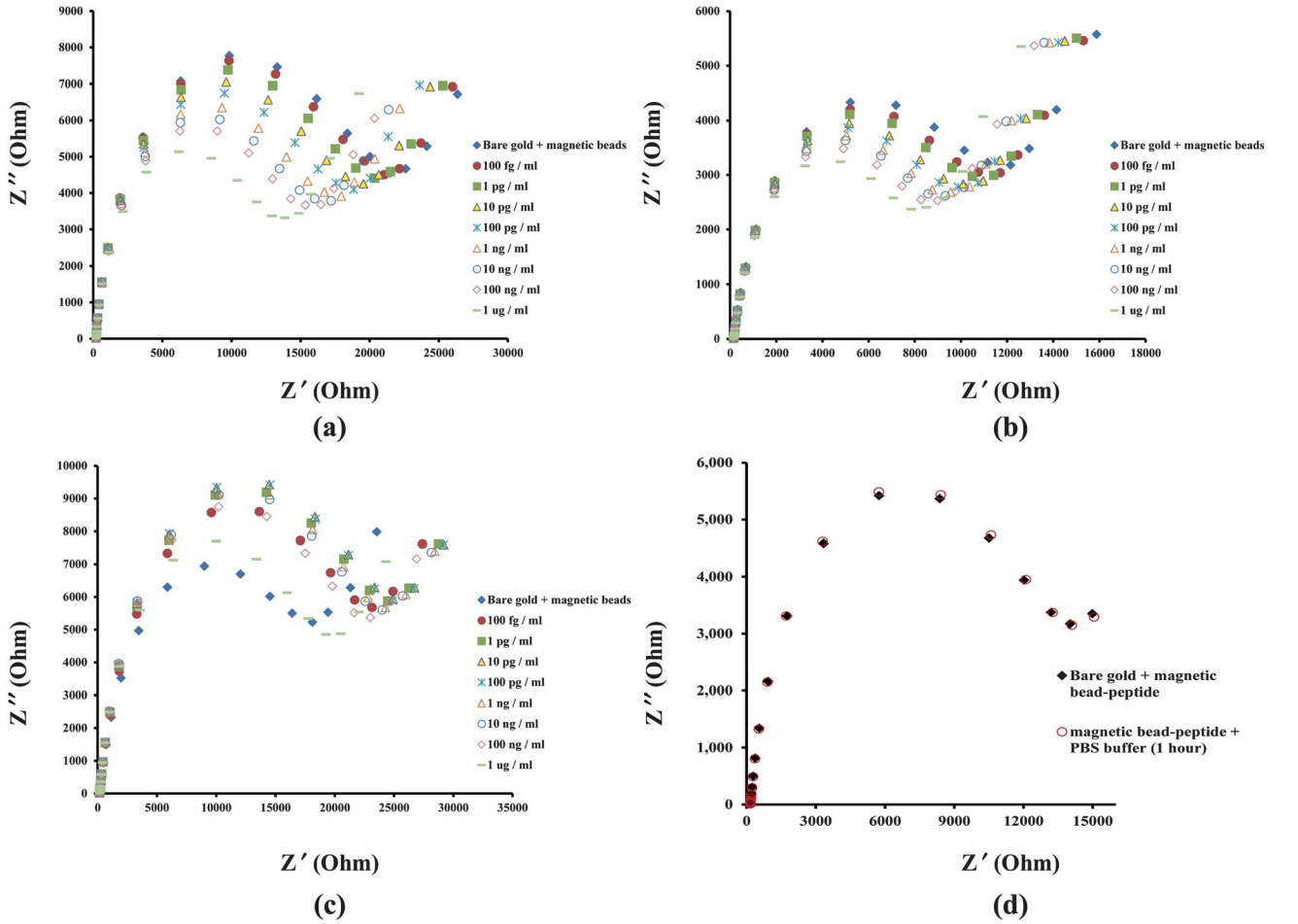

Fig. 3 PSA detection using immobilized substrate peptide 1 (a), substrate peptide 2 (b), control peptide (c) and blank experiment using PBS buffer instead of PSA solution with 1 hour incubation (d).

change in the electrochemical resistance values was observed up to one hour (Fig. 3d), indicating good stability and reliability in the operational performance of the PSA sensor.

3.2.2. Specificity of the PSA biosensor. It is important to assess the specificity of a biosensing mechanism. For this, we constructed a monolayer with a peptide non-specific to PSA (a HIV-1 protease substrate peptide lacking PSA cleavage site) and tested it with the same range of PSA concentrations. Interestingly, the results showed a gradual increase in the charge transfer resistance represented by an augmentation of the diameter of the Nyquist semi-circle (Fig. 3c). According to our previous results with the PSA-specific peptides, PSA cleavage would allow the release of magnetic beads, their subsequent attraction by an external magnet and consequently a decrease in charge transfer resistance. An increase of the impedance signal, on the other hand, could be due to the adsorption of materials on the gold surface rather than dissociation. We speculate that the PSA molecules were adsorbed non-specifically onto the bare gold surface. However, its activity is too small to such an extent that we are not able to recognize it within this huge electrochemical effect of physical adsorption. Indeed, if we look at the variation of the charge transfer resistance ($R2$) (Table 1) with different concentrations, we can see that the rate of increase in the impedimetric signal due to enzyme adsorption decreases with PSA concentration, suggesting a minor cleavage of the non-specific peptide that started to take place at higher concentrations. It is noteworthy that at 1×10^3 pg ml^{-1} of PSA, we are still able to observe an upper Nyquist plot with respect to our sensitive monolayer baseline curve. This new electrochemical behaviour is completely different from that observed when specific sequences were tested confirming that the control peptide is not cleaved by PSA and the increase in impedance is due to PSA adsorption on the sensor surface.

3.2.3. Calibration plots. Based on the theoretical charge transfer resistance values calculated for the 3 sequences, we are able to define a new parameter named charge transfer resistance variation (ΔR). ΔR corresponds to the difference in magnetic bead–peptide layer resistance before and after enzyme addition. The calibration plots ($\Delta R = f(\log[\text{PSA}])$) for substrate peptides 1 and 2 showed a linear relationship with a detection limit as low as 1 pg ml^{-1} of enzyme. On the other hand, the control non-PSA-specific peptide showed a sigmoidal dose-dependency (Fig. 4). Establishing a calibration plot will facilitate the analysis and monitoring of unknown samples in prostate cancer diagnosis. We also demonstrate in Fig. 4, the capability of the PSA biosensor to distinguish two different substrate peptides

Table 1 Values of the electrical component parameters of the equivalent circuit for the non-specific peptide

	Bare gold	Magnetic bead + peptide	100 fg ml^{-1}	1 pg ml^{-1}	10 pg ml^{-1}	100 pg ml^{-1}	1 ng ml^{-1}	10 ng ml	100 ng ml	1 μg ml^{-1}
Solution resistance *R*1 (*R*) (Ω)	186.58 (2.326%)	192.42 (0.732%)	171.50 (0.854%)	169.23 (0.869%)	169.21 (0.891%)	168.93 (0.915%)	169.96 (0.928%)	168.76 (0.933%)	169.00 (0.937%)	167.09 (0.962%)
Capacitance (CPE) *Y*0 (μS) N	—	2.7923 (2.322%) 0.83608 (0.407%)	2.6726 (2.445%) 0.84184 (0.428%)	2.5426 (2.447%) 0.84661 (0.426%)	2.4759 (2.507%) 0.85113 (0.435%)	2.4249 (2.588%) 0.85527 (0.448%)	2.3572 (2.661%) 0.85963 (0.457%)	3.2957 (2.694%) 0.86351 (0.460%)	2.2446 (2.756%) 0.86779 (0.468%)	2.1998 (2.940%) 0.87054 (0.492%)
Charge transfer resistance *R*2 (Ω)	690.23 (5.147%)	16 852 (1.334%)	21 366 (1.491%)	22 721 (1.503%)	23 144 (1.539%)	23 031 (1.578%)	22 310 (1.589%)	21 941 (1.589%)	20 780 (1.585%)	18 025 (1.605%)
Capacitance (*C*) (nF)	885.73 (5.176%)	—	—	—	—	—	—	—	—	—
Warburg diffusion (*W*) (μS)	160.86 (3.098%)	126.15 (3.965%)	141.79 (6.106%)	141.77 (6.532%)	141. 8 (6.826%)	141.35 (6.977%)	142.92 (6.949%)	142.05 (6.849%)	143.66 (6.622%)	143.15 (5.976%)

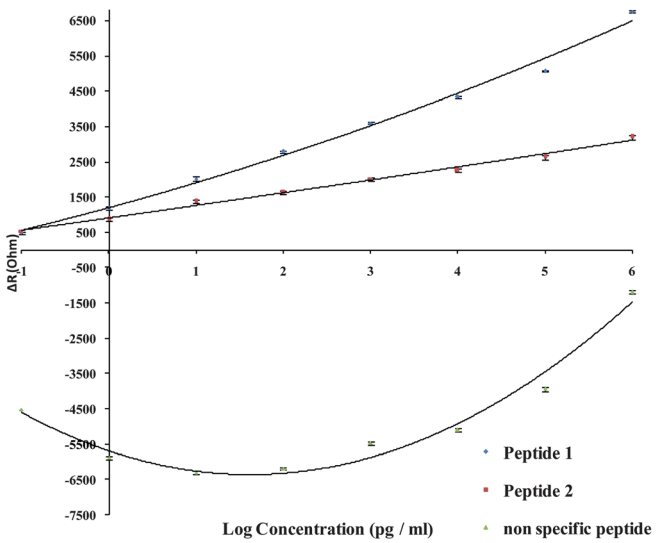

Fig. 4 Calibration plots: Δ*R* corresponds to the difference in magnetic bead–peptide layer resistance before and after enzyme addition. The error bar is corresponding to the percent relative standard deviation, and they look very small.

due to the substrate specificity of PSA and thereby the sensitivity of the biosensor. This indicates the potential application of the PSA biosensor in drug discovery. In addition, with a detection limit of 1 pg ml^{-1} of enzyme within a short analysis time (30 min), the PSA biosensor can serve as a template for further development of lab-on-a-chip devices suitable for prostate cancer diagnosis. In particular, to our knowledge, we have achieved the lowest PSA detection limit with a one-step biosensor setup. In fact, Liu *et al.*[28] were able to detect 2 × 10^3 pg ml^{-1} of PSA using horseradish peroxidase (HRP) enzyme activity as a label in order to amplify the electrochemical signal measured during PSA detection; while, Yan *et al.* recently applied the same technique (impedance spectroscopy) to detect PSA and succeeded in achieving a detection limit of 2 pg ml^{-1}. Nevertheless, these methods involved complex procedures such as labeling with HRP, as well as the introduction of gold nanoparticles as a second interface to produce a larger surface area.[29]

4. Conclusions

In this report, we described a novel and low-cost method for prostate specific antigen (PSA) detection using a monolayer of PSA substrate peptide conjugated with magnetic nano-carriers self-assembled on gold electrode surface. This configuration allows an easier manipulation of materials and eliminates complex washing and blocking steps. The application of electrochemical impedance spectroscopy (EIS) demonstrates the ability of the biosensor to analyze a wide range of PSA concentrations (from 1 pg ml^{-1} to 1 μg ml^{-1}), achieving a detection limit as low as 1 pg ml^{-1} with good specificity and reproducibility. This PSA biosensing mechanism can be integrated with other detection platforms and transducers that could potentially offer improvement in sensitivity and specificity. The present biosensing method provides very simple protease detection without washing and/or blocking steps. This unique advantage is crucial for the development of a cost-effective lab-on-a-chip device suitable for point-of-care usage.

Acknowledgements

The authors would like to acknowledge the financial support for the project given by INRS, NSERC and NanoQuebec. Also, Dr Suaifan would like to acknowledge the financial support from The University of Jordan.

References

1 T. Feng, D. Feng, W. Shi, X. Li and H. Ma, in *Molecular BioSystems*, The Royal Society of Chemistry, 2012, vol. 8, pp. 1441–1445.
2 G. Liu, M. Swierczewska, G. Niu, X. Zhang and X. Chen, *Mol. BioSyst.*, 2011, **7**, 993–1003.
3 American Cancer Society, *Cancer Facts & Figures*, Atlanta, 2010.
4 O. V. Shulga, D. Zhou, A. V. Demchenko and K. J. Stine, *Analyst*, 2008, **133**, 319–322.
5 S. P. Balk, Y.-J. Ko and G. J. Bubley, *J. Clin. Oncol.*, 2003, **21**, 383–391.
6 G. A. Suaifan, T. Arafat and M. D. Threadgill, *Bioorg. Med. Chem.*, 2007, **15**, 3474–3488.
7 S. R. Denmeade, I. Litvinov, L. J. Sokoll, H. Lilja and J. T. Isaacs, *Prostate*, 2003, **56**, 45–53.
8 C. Sun, K. H. Su, J. Valentine, Y. T. Rosa-Bauza, J. A. Ellman, O. Elboudwarej, B. Mukherjee, C. S. Craik, M. A. Shuman, F. F. Chen and X. Zhang, *ACS Nano*, 2010, **4**, 978–984.
9 P. Wu, L. Zhu, U.-H. Stenman and J. Leinonen, *Clin. Chem.*, 2004, **50**, 125–129.

10 S. R. Denmeade, W. Lou, J. Lövgren, J. Malm, H. Lilja and J. T. Isaacs, *Cancer Res.*, 1997, **57**, 4924–4930.
11 G. V. Raj, A. W. Partin and T. J. Polascik, *Cancer*, 2002, **94**, 987–996.
12 S. Sengupta, C. Amling, A. V. D'Amico and M. L. Blute, *J. Urol.*, 2008, **179**, 821–826.
13 T. K. Takayama, R. L. Vessella, M. K. Brawer, J. Noteboom and P. H. Lange, *J. Urol.*, 1993, **150**, 374–378.
14 H. Yu, E. P. Diamandis, A. F. Prestigiacomo and T. A. Stamey, *Clin. Chem.*, 1995, **41**, 430–434.
15 T. Kokko, T. Liljenbäck, M. T. Peltola, L. Kokko and T. Soukka, *Anal. Chem.*, 2008, **80**, 9763–9768.
16 J. Wang, G. Liu, H. Wu and Y. Lin, *Small*, 2008, **4**, 82–86.
17 M. Briman, E. Artukovic, L. Zhang, D. Chia, L. Goodglick and G. Gruner, *Small*, 2007, **3**, 758–762.
18 R. L. Vessella, J. Noteboom and P. H. Lange, *Clin. Chem.*, 1992, **38**, 2044–2054.
19 D. L. Woodrum, C. M. French, T. M. Hill, S. J. Roman, H. L. Slatore, J. L. Shaffer, L. G. York, K. L. Eure, K. G. Loveland, G. H. Gasior, P. C. Southwick and L. B. Shamel, *Clin. Chem.*, 1997, **43**, 1203–1208.
20 R. B. Schifman, F. R. Ahmann, A. Elvick, M. Ahmann, K. Coulis and M. K. Brawer, *Clin. Chem.*, 1987, **33**, 2086–2088.
21 R. Junker, B. Brandt, C. Zechel and G. Assmann, *Clin. Chem.*, 1997, **43**, 1588–1594.
22 C. Esseghaier, A. Ng and M. Zourob, *Biosens. Bioelectron.*, 2012, DOI: 10.1016/j.bios.2012.08.049.
23 M. G. Silva, S. Helali, C. Esseghaier, C. E. Suarez, A. Oliva and A. Abdelghani, *Sens. Actuators, B*, 2008, **135**, 206–213.
24 H. B. Fredj, S. Helali, C. Esseghaier, L. Vonna, L. Vidal and A. Abdelghani, *Talanta*, 2008, **75**, 740–747.
25 C. Esseghaier, S. Helali, H. B. Fredj, A. Tlili and A. Abdelghani, *Sens. Actuators, B*, 2008, **131**, 584–593.
26 L. H. Dubois and R. G. Nuzzo, *Annu. Rev. Phys. Chem.*, 1992, **43**, 437.
27 C. Esseghaier, Y. BergaouI, H. ben Fredj, A. Tlili, S. Helali, S. Ameur and A. Abdelghani, *Sens. Actuators, B*, 2008, **134**, 112–118.
28 S. Liu, X. Zhang, Y. Wu, Y. Tu and L. He, *Clin. Chim. Acta*, 2008, **395**, 51–56.
29 M. Yan, D. Zang, S. Ge, L. Ge and J. Yu, *Biosens. Bioelectron.*, 2012, **38**, 355–361.